Computers and Geotechnics 35 (2008) 845–852

Contents lists available at ScienceDirect

Computers and Geotechnics

journal homepage: www.elsevier.com/locate/compgeo

Elastoplastic prediction of hydro-mechanical behaviour of unsaturated soils under undrained conditions

De'An Sun [a,*], Daichao Sheng [b], Li Xiang [a], Scott W. Sloan [b]

[a] Department of Civil Engineering, Shanghai University, 149 Yanchang Road, Shanghai 200072, China
[b] Centre for Geotechnical and Materials Modelling, School of Engineering, The University of Newcastle, Callaghan, NSW 2308, Australia

ARTICLE INFO

Article history:
Available online 14 September 2008

Keywords:
Unsaturated soil
Undrained soil behaviour
Elastoplastic model
Soil–water characteristic behaviour

ABSTRACT

A number of hydro-mechanical elastoplastic constitutive models for unsaturated soils have recently been proposed. These models couple the hydraulic and mechanical behaviour of unsaturated soils, and take into account the effects of the degree of saturation on the stress–strain behaviour and the effects of deformation on the soil–water characteristic response. In addition, the influence of the suction on the stress–strain behaviour is considered. However, until now, there is no model that predicts the stress–strain and soil–water characteristic responses of unsaturated soils under undrained conditions or constant gravimetric water contents. This paper presents the predictions of an unsaturated soil model for undrained conditions, and compares these predictions with experimental results obtained from undrained isotropic compression and triaxial compression tests on an unsaturated compacted soil. It is shown that the model predicts the hydraulic and mechanical behaviour of unsaturated soil accurately under undrained conditions.

1. Introduction

Elastoplastic constitutive modelling for unsaturated soils was pioneered by Alonso et al. [1] and Gens et al. [4], whose work led to the complete formulation of Alonso et al. [2]. Since then, a number of constitutive relations have been proposed which are based on experimental and theoretical studies (e.g., [6,13,5,9]. In recent years, some elastoplastic constitutive formulations have also incorporated hydraulic hysteresis of the soil–water characteristic into the stress–strain behaviour (e.g., [3,12,14,7,10]. These models describe the mechanical and hydraulic behaviour of unsaturated soils simultaneously. However, until now, no hydro-mechanical simulations of unsaturated soil behaviour during loading under undrained conditions or constant gravimetric water content have been reported. Since the elastoplastic constitutive relations for saturated soils can be formulated using effective stresses, their undrained response can be predicted by imposing the constant volume condition even though the effective stress path is not given during loading. Similarly, the undrained condition for an unsaturated soil in this paper refers to the situation of constant gravimetric water content in the soil. Constant gravimetric water content can be achieved by closing all water drains during a test. It is also an additional constraint in constitutive modelling and can be used to predict the soil behaviour without the need to specify the suction during loading.

In this paper, we first briefly review a hydro-mechanical elastoplastic model for unsaturated soils proposed by the authors [10]. Next, using this model, the equations for predicting the undrained hydraulic and stress–strain behaviour of unsaturated soils are formulated. Finally, the model predictions are compared with the experimental results of isotropic compression and triaxial shear tests on an unsaturated compacted soil under undrained conditions.

2. Elastoplastic model incorporating soil–water characteristic behaviour

The elastoplastic constitutive model for unsaturated soils proposed by the authors [10] incorporates the influence of the degree of saturation on the stress–strain relations and strength, the influence of deformation on the soil–water characteristic response, and the influence of suction on both types of behaviour. The model is applicable to unsaturated soils in which the pore air and pore water are continuous throughout the voids. This paper adopts the model to simulate the hydraulic and mechanical behaviour of unsaturated soil under undrained conditions. In this section, the model is reviewed briefly.

2.1. Stress-state variables for unsaturated soils

To identify the hydraulic and mechanical behaviour of unsaturated soils properly, the stress-state variables employed in the

* Corresponding author. Tel.: +86 21 56334259; fax: +86 21 56331971.
E-mail address: sundean@hotmail.com (D.A. Sun).

0266-352X/$ - see front matter © 2008 Elsevier Ltd. All rights reserved.
doi:10.1016/j.compgeo.2008.08.002

model are the 'average skeleton' stress tensor σ'_{ij} and suction s, while the strain-state variables are the soil skeleton strain tensor ε_{ij} and the degree of saturation S_r. The average skeleton tensor σ'_{ij} is defined by

$$\sigma'_{ij} = \sigma_{ij} - u_a\delta_{ij} + S_r s\delta_{ij} \tag{1}$$

where σ_{ij} is the total stress tensor, u_a is the pore-air pressure, and δ_{ij} is the Kronecker delta. The average skeleton stress and suction variables adopted in the model permit a general form of hydraulic behaviour to be represented and also provide a smooth transition between the saturated and unsaturated states.

2.2. Soil–water characteristic behaviour of unsaturated soil

An important feature of unsaturated soil behaviour is the irreversible change in volume and degree of saturation that is caused by cyclic drying and wetting under constant net stress. After examining many isotropic and triaxial compression test results for unsaturated compacted soils during wetting, we concluded that the degree of saturation is mainly dependent on the wetting-drying history, suction and void ratio, and is not directly dependent on the stress-state for a given soil [11]. Therefore, the equations identifying the soil–water characteristic curve can be simply idealized as shown in Fig. 1.

The main drying and main wetting curves of the soil–water characteristic curves are expressed respectively by

$$\begin{aligned} S_r &= S^0_{rd}(e) - \lambda_{sr}\ln s \quad \text{main drying} \\ S_r &= S^0_{rw}(e) - \lambda_{sr}\ln s \quad \text{main wetting} \end{aligned} \tag{2}$$

while a scanning curve is given as

$$S_r = S^0_{rs}(e) - \kappa_s \ln s \tag{3}$$

In these equations, λ_{sr} and κ_s are the slopes of the main drying (or wetting) curve and the scanning curve, respectively; $S^0_{rd}(e)$ and $S^0_{rw}(e)$ are the degrees of saturation respectively on the main drying and main wetting curve when $s = 1$, and is a function of the void ratio e, $S^0_{rs}(e)$ is the degree of saturation on the specific scanning curve when $s = 1$, and is also a function of the void ratio e. The values of $S^0_{rd}(e), S^0_{rw}(e)$ and $S^0_{rs}(e)$ will depend on the void ratio and the unit chosen for the suction measurement. Throughout this paper it is assumed that the unit of suction is 1 kilopascal (kPa).

According to the results of isotropic compression tests and triaxial tests on unsaturated soils under constant suction, the void ratio versus degree of saturation relation under constant suction can be approximated by [10]:

$$\mathrm{d}S^0_{ri}(e) = -\lambda_{se}\mathrm{d}e, \qquad i = d, w, s \tag{4}$$

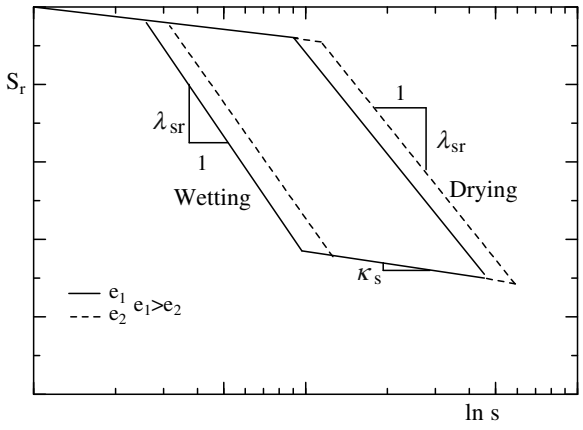

Fig. 1. Model for soil–water characteristic curves at different void ratios.

where λ_{se} is the slope of the S_r–e curve under constant suction. Differentiating Eqs. (2) and (3) and then combining them with Eq. (4) lead to

$$\mathrm{d}S_r = -\lambda_{se}\mathrm{d}e - \lambda_{sr}\frac{\mathrm{d}s}{s} \tag{5}$$

$$\mathrm{d}S_r = -\lambda_{se}\mathrm{d}e - \kappa_s\frac{\mathrm{d}s}{s} \tag{6}$$

The above equations define the incremental soil–water characteristic relations of unsaturated soils.

2.3. Formulation of the model for isotropic stress states

The so-called load-collapse (LC) yield curve in the p–s plane under an isotropic stress-state can be modelled using the following equation:

$$p'_y = p'_n\left(\frac{p_{0y}}{p'_n}\right)^{\frac{\lambda(0)-\kappa}{\lambda(s)-\kappa}} \tag{7}$$

where p_{0y} and p'_y are the yield stresses for saturated soil and unsaturated soil with suction s (see Fig. 2), p'_n is an isotropic stress at which no collapse occurs when the suction is decreased, κ is a swelling index for unsaturated soils (including saturated soil in the e–$\ln p'$ plane), and $\lambda(0)$ and $\lambda(s)$ are the slopes of the normal compression lines of saturated soil and unsaturated soil with suction s in the e–$\ln p'$ plane. The quantity $\lambda(s)$ is assumed to take the form:

$$\lambda(s) = \lambda(0) + \frac{\lambda_s s}{p_a + s} \tag{8}$$

where λ_s is a material parameter and $\lambda(0) + \lambda_s$ represents the slope of the e–$\ln p'$ curve when the suction approaches infinite. The slope $\lambda(s)$ is assumed to increase with increasing suction, so that the wetting-induced collapse does not increase with increasing mean stress (see [9]). From Eq. (7), we have:

$$\mathrm{d}p'_y = \frac{\partial p'_y}{\partial p_{0y}}\mathrm{d}p_{0y} + \frac{\partial p'_y}{\partial s}\mathrm{d}s \tag{9}$$

where

$$\frac{\partial p'_y}{\partial p_{0y}} = \frac{\lambda(0)-\kappa}{\lambda(s)\kappa}\left(\frac{p_{0y}}{p'_n}\right)^{\frac{\lambda(0)-\lambda(s)}{\lambda(s)-\kappa}} \tag{10}$$

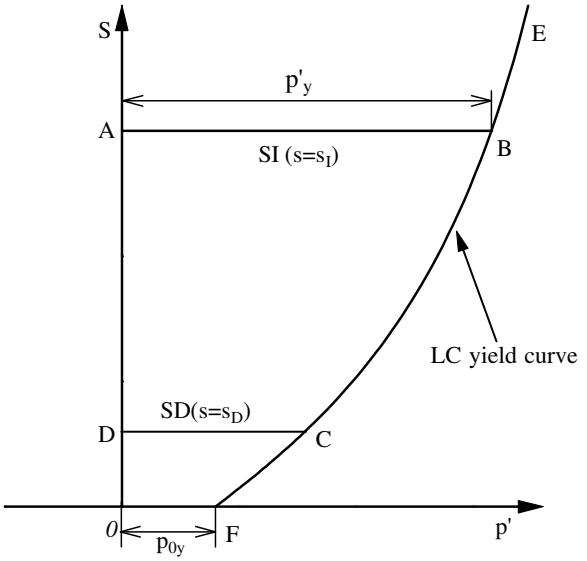

Fig. 2. LC yield curve, SI and SD yield curves for isotropic stress states.

$$\frac{\partial p'_y}{\partial s} = \frac{\lambda_s p'_n p_a (\lambda(0)-\kappa)}{(\lambda(s)-\kappa)^2 (p_a+s)^2} \ln\left(\frac{p'_n}{p_{0y}}\right) \tag{11}$$

When the stress-state is inside the LC yield curve, the elastic volumetric strain increment is given by

$$d\varepsilon_v^e = \frac{\kappa dp'}{(1+e)p'} \tag{12}$$

where p' is an isotropic average skeleton stress.When the stress-state is on the LC yield curve, the plastic volumetric strain increment is given by

$$d\varepsilon_v^p = \frac{(\lambda(0)-\kappa)dp_{0y}}{(1+e)p_{0y}} \tag{13}$$

In addition to the LC yield curve, two more yield curves are needed to model hydraulic hysteresis as an elastoplastic process (see Fig. 2). The soil–water characteristic behaviour shown in Fig. 1 is represented by a suction increase (SI) yield curve and a suction decrease (SD) yield curve in the p'–s plane. When the suction changes during a drying ($s \geqslant s_I$) or wetting ($s \leqslant s_D$) process, the degree of saturation increment is given by Eq. (5); otherwise, the degree of saturation increment is given by Eq. (6). Therefore, according to the relation between the stress-state (p' and s) and the yield curves (LC, SI, and SD), different equations must be used to calculate the strains and the degree of saturation. When $dp_{0y} > 0$ and $s > s_I$ or $s < s_D$, the volumetric strain and the degree of saturation are calculated using Eqs. (12), (13), and (5). When $dp_{0y} > 0$ and $s_D \leqslant s \leqslant s_I$, these quantities are calculated from Eqs. (12), (13), and (6). When $dp_{0y} = 0$, and $s > s_I$ or $s < s_D$, the volumetric strain and the degree of saturation are calculated using Eqs. (12) and (5). When $dp_{0y} = 0$ and $s_D \leqslant s \leqslant s_I$, they are found from Eqs. (12) and (6).

2.4. Formulation of the model under triaxial stress states

Assuming an associated flow rule, the yield function (f) and the plastic potential function (g) are proposed to have the following form:

$$f = g = q^2 + M^2 p'(p' - p'_y) = 0 \tag{14}$$

where M is the slope of the critical line in the p'-q plane. Fig. 3 shows the geometry of the yield function for $s > 0$ (the unsaturated state) and $s = 0$ (the saturated state) in the p'–q plane.

The associated flow rule is obeyed in terms of the average skeleton stress space according to

$$d\varepsilon_{ij}^p = \Lambda \frac{\partial f}{\partial \sigma'_{ij}} \tag{15}$$

where the proportionality constant Λ can be determined from the consistency condition. Since Eq. (14) can be rewritten as $f = f(p', q, p'_y) = 0$, we have:

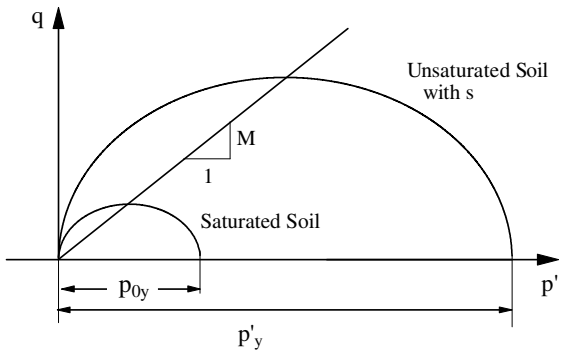

Fig. 3. Yield curves under constant suctions.

$$df = \frac{\partial f}{\partial p'}dp' + \frac{\partial f}{\partial q}dq + \frac{\partial f}{\partial p'_y}dp'_y = 0 \tag{16}$$

Substituting Eq. (9) into Eq. (16) and re-arranging gives:

$$df = \frac{\partial f}{\partial p'}dp' + \frac{\partial f}{\partial q}dq + \frac{\partial f}{\partial p'_y}\frac{\partial p'_y}{\partial p_{0y}}dp_{0y} + \frac{\partial f}{\partial p'_y}\frac{\partial p'_y}{\partial s}ds = 0 \tag{17}$$

where the isotropic yielding stress p_{0y} for saturated soil is related to the volumetric strain ε_v^p. Because the plastic volumetric strain ε_v^p is a hardening parameter in the model, the volumetric plastic strains $d\varepsilon_v^p$ caused by dp_{0y} in a saturated soil are the same as those in an unsaturated soil which are caused by dp_{0y} and/or ds. Combining Eqs. (13) and (15) gives:

$$dp_{0y} = \frac{1+e}{\lambda(0)-\kappa}p_{0y}d\varepsilon_v^p = \frac{1+e}{\lambda(0)-\kappa}p_{0y}\Lambda\frac{\partial f}{\partial p'} \tag{18}$$

Substituting Eq. (18) into Eq. (17) and solving for Λ gives:

$$\Lambda = -\frac{\frac{\partial f}{\partial p'}dp' + \frac{\partial f}{\partial q}dq + \frac{\partial f}{\partial p'_y}\frac{\partial p'_y}{\partial s}ds}{\frac{\partial f}{\partial p'_y}\frac{\partial p'_y}{\partial p_{0y}}p_{0y}\frac{1+e}{\lambda(0)-\kappa}\frac{\partial f}{\partial p'}} \tag{19}$$

From Eqs. (15) and (19), it is possible to calculate the plastic strain increments caused by an increment in the average skeleton stress and/or the decrement in suction.

3. Modelling of unsaturated soil behavior under undrained conditions

In the above elastoplastic model for unsaturated soils, we need to know the average skeleton stress and suction to predict deformation and degree of saturation. If the stress paths are specified in terms of the net stress σ_{ij}–$u_a\delta_{ij}$ and suction s, the increments in σ'_{ij} are found by differentiating Eq. (1) according to

$$d\sigma'_{ij} = d(\sigma_{ij} - u_a\delta_{ij}) + (S_r ds + s dS_r)\delta_{ij} \tag{20}$$

In order to express the soil water characteristic curve simply, Eqs. (5) and (6) can be written as

$$dS_r = -\lambda_{se}de - \beta\frac{ds}{s} \tag{21}$$

where

$$\beta = \begin{cases} \kappa_s & \text{for the scanning curve} \\ \lambda_{sr} & \text{for the main wetting or drying curve} \end{cases} \tag{22}$$

Substituting Eq. (21) into Eq. (20) gives

$$d\sigma'_{ij} = d(\sigma_{ij} - u_a\delta_{ij}) + [(S_r - \beta)ds - \lambda_{se}s de]\delta_{ij} \tag{23}$$

For undrained tests on unsaturated soil we only know the net stress paths, the initial suction, the initial degree of saturation, and the gravimetric water content of the specimen. As mentioned before, to predict the deformation and degree of saturation we need to know the average skeleton stress and the suction. In the following, we formulate the equations to obtain the average skeleton stress and suction from the known net stress path for isotropic stress and triaxial stress states under undrained conditions.

3.1. Formulation for an isotropic stress-state

From Eq. (23), we know that $d\sigma'_{ij}$ is related to de and ds, in addition to the net stress σ_{ij}–$u_a\delta_{ij}$. For undrained conditions $eS_r = wG_S$= constant, where w is the gravimetric water content and G_s is specific gravity. During loading and/or wetting/drying under constant gravimetric water content, we have:

$$e dS_r = -S_r de \tag{24}$$

Combining Eq. (21) into Eq. (24) gives

$$\frac{S_r}{e} - \lambda_{se} = \frac{\beta \mathrm{d}s}{s\mathrm{d}e} \tag{25}$$

When the stresses lie inside the LC yield curve for an isotropic stress-state:

$$\mathrm{d}e = -\frac{\kappa \mathrm{d}p'}{p'} \tag{26}$$

where p' is an isotropic average skeleton stress.

Substituting Eq. (26) into Eq. (23) and rearranging gives

$$\mathrm{d}p' = \frac{\mathrm{d}p_{\mathrm{net}} + (S_r - \beta)\mathrm{d}s}{p' - s\kappa\lambda_{se}} p' \tag{27}$$

where p_{net} is an isotropic net stress.

Substituting Eq. (27) into Eq. (26) gives

$$\mathrm{d}e = \frac{\kappa[\mathrm{d}p_{\mathrm{net}} + (S_r - \beta)\mathrm{d}s]}{s\kappa\lambda_{se} - p'} \tag{28}$$

Inserting Eq. (28) into Eq. (25) and rearranging gives

$$\mathrm{d}s = \frac{s\kappa(S_r - \lambda_{\mathrm{se}}e)\mathrm{d}p_{\mathrm{net}}}{\beta e(s\kappa\lambda_{\mathrm{se}} - p') + s\kappa(S_r - \beta)(\lambda_{\mathrm{se}}e - S_r)} \tag{29}$$

When only elastic deformation takes place for an isotropic stress-state under undrained conditions, ds can be calculated from Eq. (29) using the value of dp_{net}; dp' and de can be calculated from Eqs. (27) and (28), respectively, using the values of ds and dp_{net}; dS_r can be calculated from Eq. (21) using the values of ds and de.

When the stresses lie on the LC yield curve for an isotropic stress-state:

$$\mathrm{d}e = -\frac{\lambda(0)\mathrm{d}p_{0y}}{p_{0y}} \tag{30}$$

Substituting Eq. (30) into Eq. (23) gives

$$\mathrm{d}p'_y = \mathrm{d}p_{\mathrm{net}} + (S_r - \beta)\mathrm{d}s + \frac{\lambda_{se}\lambda(0)s\mathrm{d}p_{0y}}{p_{0y}} \tag{31}$$

where p_{net} is an isotropic net stress corresponding to the average skeleton stress p'_y. Rearranging Eq. (9) gives

$$\mathrm{d}p_{0y} = \frac{\mathrm{d}p'_y - \frac{\partial p'_y}{\partial s}\mathrm{d}s}{\frac{\partial p'_y}{\partial p_{0y}}} \tag{32}$$

Inserting Eq. (31) into Eq. (32), and rearranging gives

$$\mathrm{d}p_{0y} = \frac{\mathrm{d}p_{\mathrm{net}} + \left(S_r - \beta - \frac{\partial p'_y}{\partial s}\right)\mathrm{d}s}{\frac{\partial p'_y}{\partial p_{0y}} - \frac{\lambda_{se}\lambda(0)s}{p_{0y}}} \tag{33}$$

while Eqs. (33) and (30) furnish

$$\mathrm{d}e = \frac{\lambda(0)\left[\mathrm{d}p_{\mathrm{net}} + \left(S_r - \beta - \frac{\partial p'_y}{\partial s}\right)\right]\mathrm{d}s}{\lambda_{se}\lambda(0)s - p_{0y}\frac{\partial p'_y}{\partial p_{0y}}} \tag{34}$$

Combining Eq. (34) into Eq. (25) and rearranging gives

$$\mathrm{d}s = \frac{s\lambda(0)(S_r - \lambda_{se}e)\mathrm{d}p_{\mathrm{net}}}{\beta e\left[\lambda_{se}\lambda(0)s - p_{0y}\frac{\partial p'_y}{\partial p_{0y}}\right] - s\lambda(0)(S_r - \lambda_{se}e)\left(S_r - \beta - \frac{\partial p'_y}{\partial s}\right)} \tag{35}$$

When elastoplastic deformation takes place for an isotropic stress-state under undrained conditions, ds can be calculated from Eq. (35) using the value of dp_{net}; dp_{0y} can be calculated from Eq. (33) using the values of dp_{net} and ds, and de can be calculated from Eq. (30) using the value of dp_{0y}; dS_r can be calculated from Eq. (21) using the values of ds and de.

3.2. Formulation for a triaxial stress-state

When the stresses lie inside the yield surface under a triaxial stress-state:

$$\mathrm{d}e = -\frac{\kappa \mathrm{d}p'}{p'} \tag{36}$$

Combining Eq. (36) into Eq. (23) and rearranging gives

$$\mathrm{d}p' = \frac{\mathrm{d}p_{\mathrm{net}} + (S_r - \beta)\mathrm{d}s}{p' - s\kappa\lambda_{se}} p' \tag{37}$$

where p_{net} is the mean net stress.

Substituting Eq. (37) into Eq. (36) gives

$$\mathrm{d}e = \frac{\kappa[\mathrm{d}p_{\mathrm{net}} + (S_r - \beta)\mathrm{d}s]}{s\kappa\lambda_{se} - p'} \tag{38}$$

while Eq. (38) and Eq. (25) lead to

$$\mathrm{d}s = \frac{s\kappa(S_r - \lambda_{\mathrm{se}}e)\mathrm{d}p_{\mathrm{net}}}{\beta e(s\kappa\lambda_{\mathrm{se}} - p') + s\kappa(S_r - \beta)(\lambda_{\mathrm{se}}e - S_r)} \tag{39}$$

When only elastic deformation takes place for a triaxial stress-state under undrained conditions, ds can be calculated from Eq. (39) using the value of dp_{net}; dp' and de can be found from Eqs. (37) and (38), respectively, using the values of ds and dp_{net}; dS_r is given by Eq. (21) using the values of ds and de.

When the stresses lie on the yield surface for a triaxial stress-state, differentiation of Eq. (14) leads to

$$\mathrm{d}p'_y = \left(2 - \frac{p'_y}{p'}\right)\mathrm{d}p' + \frac{2q}{M^2 p'}\mathrm{d}q \tag{40}$$

Manipulating Eqs. (23), (40), and (30) gives

$$\mathrm{d}p'_y = \left(2 - \frac{p'_y}{p'}\right)\left[\mathrm{d}p_{\mathrm{net}} + (S_r - \beta)\mathrm{d}s + \frac{s\lambda_{se}\lambda(0)}{p_{0y}}\mathrm{d}p_{0y}\right] + \frac{2q}{M^2 p'}\mathrm{d}q \tag{41}$$

while Eqs. (41) and (32) furnish

$$\mathrm{d}p_{0y} = \frac{(2p' - p'_y)\mathrm{d}p_{\mathrm{net}} + \left[(S_r - \beta)(2p' - p'_y) - p'\frac{\partial p'_y}{\partial s}\right]\mathrm{d}s + \frac{2q}{M^2}\mathrm{d}q}{p'\frac{\partial p'_y}{\partial p_{0y}} - 2(p' - p'_y)\frac{\lambda_{se}\lambda(0)s}{p_{0y}}} \tag{42}$$

Substituting Eq. (42) into Eq. (30) gives

$$\mathrm{d}e = \frac{\lambda(0)\left\{(2p' - p'_y)\mathrm{d}p_{\mathrm{net}} + \left[(S_r - \beta)(2p' - p'_y) - p'\frac{\partial p'_y}{\partial s}\right]\mathrm{d}s + \frac{2q}{M^2}\mathrm{d}q\right\}}{(2p' - p'_y)\lambda_{se}\lambda(0)s - p_{0y}p'\frac{\partial p'_y}{\partial p_{0y}}} \tag{43}$$

while inserting Eq. (43) into Eq. (25) and rearranging furnishes

$$\mathrm{d}s = \frac{\left(\frac{S_r}{e} - \lambda_{se}\right)s\lambda(0)\left[(2p' - p'_y)\mathrm{d}p_{\mathrm{net}} + \frac{2q}{M^2}\mathrm{d}q\right]}{\beta\left[(2p' - p'_y)\lambda_{se}\lambda(0)s - p_{0y}p'\frac{\partial p'_y}{\partial p_{0y}}\right] + \left(\lambda_{se} - \frac{S_r}{e}\right)s\lambda(0)\left[(S_r - \beta)(2p' - p'_y) - p'\frac{\partial p'_y}{\partial s}\right]} \tag{44}$$

When elastoplastic deformation takes place for a triaxial stress-state under undrained conditions, ds can be found from Eq. (44) using the value of dp_{net} and dq; dp_{0y} can be calculated from Eq. (42) using the values of dp_{net}, dq and ds, and de can be computed from Eq. (30) using the value of dp_{0y}. dS_r can be found from Eq. (21) using the values of ds and de.

The elastic component is calculated from Hooke's law using the average skeleton stress instead of the net stress and suction, where the increments in the former are calculated from Eq. (23). Poisson's ratio is assumed to be 1/3 and the elastic modulus is calculated from Eq. (36):

$$E = \frac{p'(1+e)}{\kappa} \tag{45}$$

4. Comparison of model predictions with experimental results

4.1. Undrained tests on unsaturated soil

In order to observe undrained unsaturated soil behaviour, an isotropic compression test and two triaxial compression tests on unsaturated compacted Pearl clay were carried out under constant gravimetric water content conditions. Details of the clay properties, specimen preparation, and triaxial testing apparatus for unsaturated soils can be found in Sun et al. [8–11]. The previous tests on unsaturated Pearl clay were performed with the net stress and suction paths being controlled, with the strains (including the axial strain and lateral strain) and water content being measured, i.e., so-called drained tests. In the present work, the tests on the same unsaturated compacted clay were performed with the net stress path being controlled and with the suction and the strains being measured under constant gravimetric water content (i.e., closing the drainage valve for pore water), i.e., undrained tests here. The pore water pressure was measured with the pore air pressure being kept at a constant value during the testing, i.e., the suction was not controlled but measured during the test.

4.2. Model parameters

As discussed in [10], the model requires five material parameters to describe the stress–strain behaviour ($\lambda(0), \lambda_s, \kappa, p'_n, M$) and three material parameters to describe the soil–water characteristic behaviour ($\lambda_{sr}, \kappa_s, \lambda_{se}$).

The values of the material parameters that were used to predict the stress–strain and soil–water characteristic behaviour of the Pearl clay are as follows: $\lambda(0) = 0.11$, $\kappa = 0.03$, $\lambda_s = 0.13$, $p'_n = 1.62$ MPa, $M = 1.1$, $\lambda_{se} = 0.35$, $\lambda_{sr} = 0.13$, $\kappa_s = 0.03$.

These values are the same as those used to predict the stress–strain and soil–water characteristic behaviour under drained conditions (see Fig. 4). In addition to the above-mentioned model parameters, the initial state values – including initial suction (s_0), initial void ratio (e_0), initial degree of saturation (S_{r0}), and initial yield stress p_{0y} – are needed for the model predictions.

4.3. Model predictions versus experimental results

Fig. 4 shows the measured and predicted results of triaxial compression tests on compacted Pearl clay under drained condition, i.e., with the net stress and suction being controlled ($p = 196$ kPa and $s = 100$ kPa) and the strains and water content being measured. In the figure, σ_1/σ_3 is the net stress ratio, and ε_1, ε_3 and ε_v are the axial strain, lateral strain and volumetric strain, respectively. The model parameters used for the prediction in Fig. 4 include: the initial state values of $e_0 = 1.11$, $S_{r0} = 76.0\%$, and $p_{0y} = 40$ kPa, in additional to those material parameters given above. From Fig. 4, it can be seen that the model by Sun et al. [10] is capable of predicting the stress–strain relation as well as the variation of the degree of saturation under drained condition.

Fig. 5 shows the measured and predicted results of the isotropic compression test on unsaturated compacted Pearl clay, under undrained conditions, in terms of the relations: (a) void ratio versus mean net stress, (b) void ratio versus suction, (c) degree of saturation versus mean net stress, and (d) degree of saturation versus suction, i.e., soil–water characteristic curve. The isotropic net stress was applied from 20 kPa to 600 kPa under undrained conditions, with the pore water pressure being measured and the pore air pressure being kept at 100 kPa during loading. Fig. 6 shows the measured and predicted stress paths of the same test during the isotropic compression under undrained conditions, in terms of (a) suction versus mean net stress relation, and (b) suction versus mean average skeleton stress. The collapse-loading (LC) yield curves corresponding to the initial and final states are also shown in Fig. 6b. The test results show that with the increase in the mean net stress p_{net}, the pore water pressure u_w also increases. Since the pore air pressure u_a was kept unchanged ($u_a = 100$ kPa), the suction s decreases with the compression. Note also that the volume decreases with increasing isotropic compression stress for unsaturated soil, which is a significant difference from the undrained test on saturated soil.

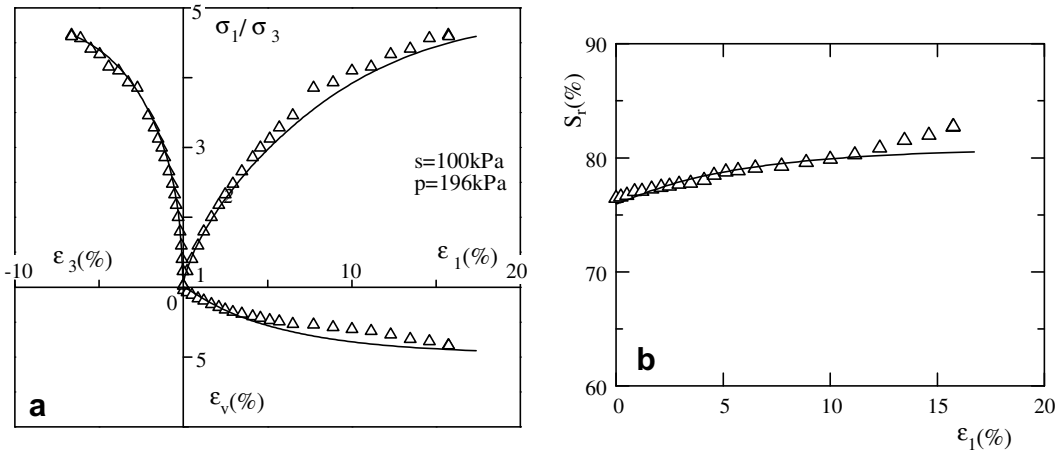

Fig. 4. Predicted and measured results of triaxial compression test on unsaturated Pearl clay under $s = 100$ kPa and $p = 196$ kPa.

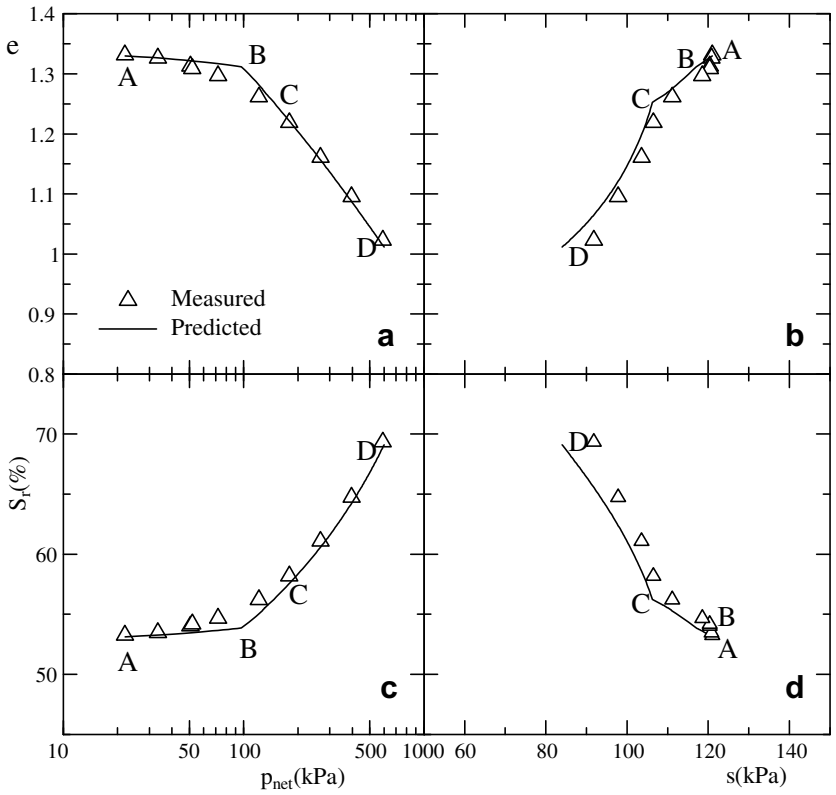

Fig. 5. Measured and predicted results of isotropic compression test on unsaturated Pearl clay under undrained condition.

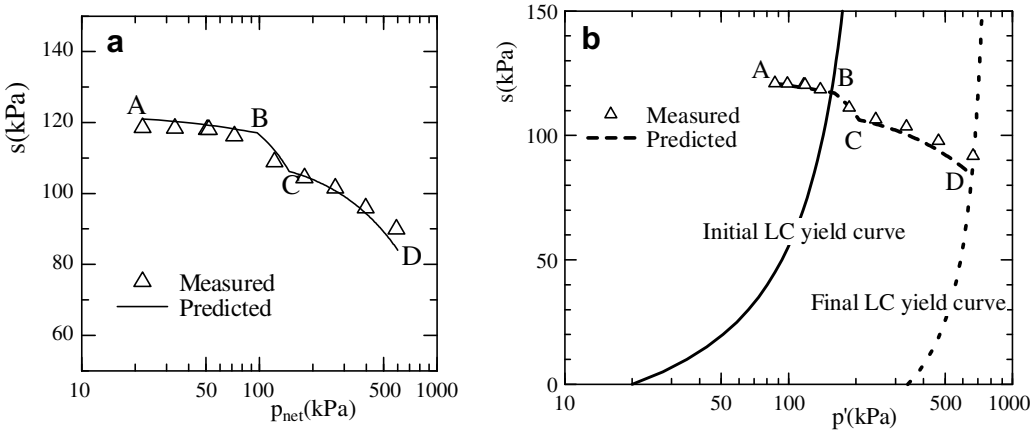

Fig. 6. Measured and predicted stress paths during isotropic loading under undrained condition.

Initial state values of $s_0 = 120$ kPa, $e_0 = 1.33$, $S_{r0} = 52.5\%$, and $p_{0y} = 20$ kPa were observed at the beginning of the test, and these values were used as the initial values in the model predictions in Figs. 5 and 6. The test and predicted results show that the suction decreases and the degree of saturation increases during isotropic compression under undrained conditions. It can be seen that the model provides good predictions of the stress–strain and soil–water characteristic behaviour of unsaturated compacted clay during the isotropic compression. The changes in the void ratio, degree of saturation, and suction are relatively small during isotropic loading over the Section AB, because the deformation and hydraulic characteristics are "elastic". In Section BC, the deformation is elastoplastic but the hydraulic characteristics are still "elastic". In Section CD, the changes in the void ratio, degree of saturation, and suction are larger because the deformation and hydraulic characteristics are "elastoplastic". Overall, the model predictions are in agreement with the test results.

Figs. 7 and 8 compare the measured and predicted results for undrained triaxial compression tests on unsaturated compacted Pearl clay with a different suction and degree of saturation prior to shearing, although the initial state of the specimens is almost the same as that for Figs. 5 and 6. Unlike undrained tests on saturated soil, volume change takes place during undrained shear tests on unsaturated clay.

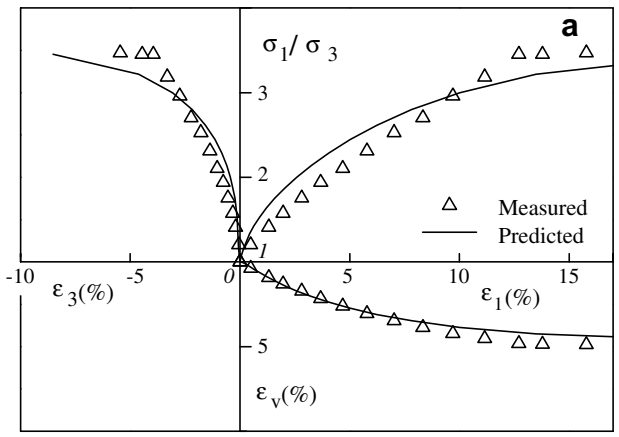

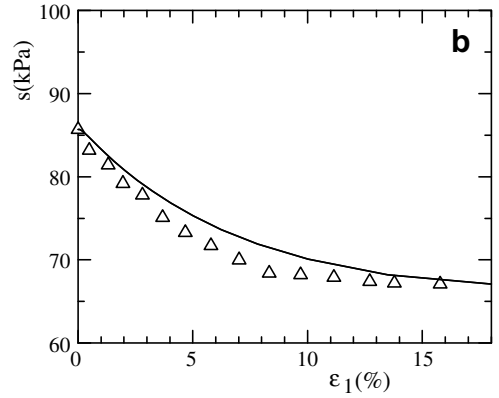

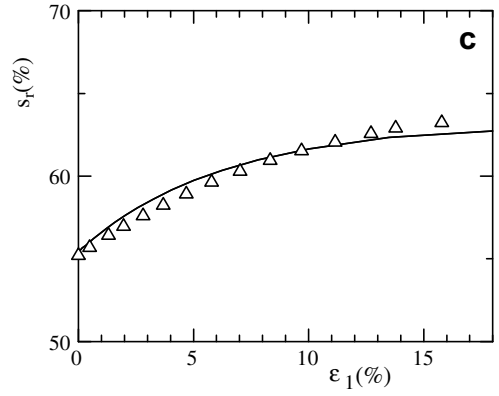

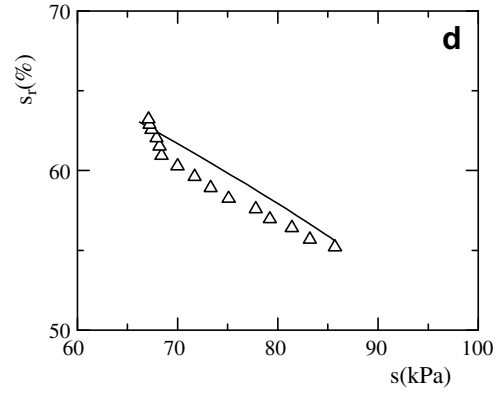

Fig. 7. Measured and predicted (a) stress–strain, (b) suction versus axial strain, (c) degree of saturation versus axial strain, and (d) degree of saturation versus suction relations from undrained triaxial test on compacted clay at relatively low degree of saturation under constant mean net stress (p_{net} = 200 kPa).

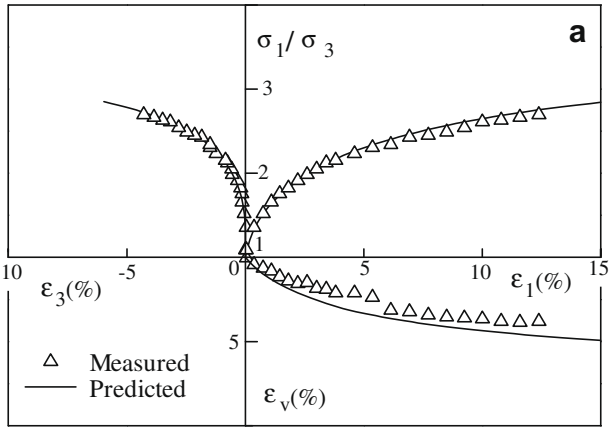

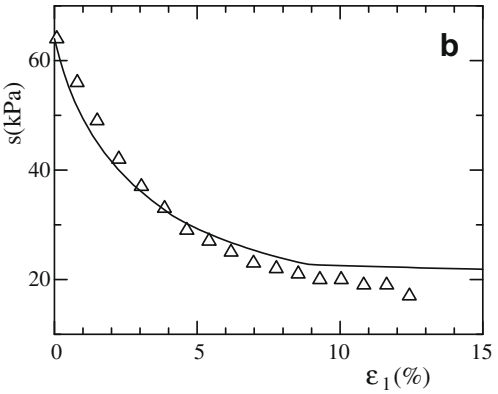

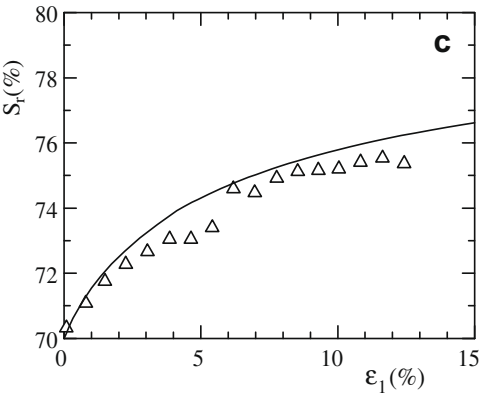

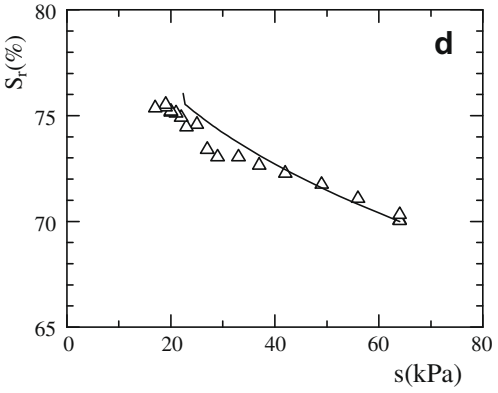

Fig. 8. Measured and predicted (a) stress–strain, (b) suction versus axial strain, (c) degree of saturation versus axial strain, and degree of saturation versus suction relations from undrained triaxial test at relatively high degree of saturation under constant net confining stress σ_3 = 100 kPa.

Fig. 7 shows the predicted and measured results for an undrained triaxial compression test on unsaturated compacted Pearl clay with a relatively low initial degree of saturation. During the testing, a constant mean net stress (p_{net} = 200 kPa) was applied to the specimen. The initial values of s_0 = 85.4 kPa, e_0 = 1.23, S_{r0} = 55.2% and p_{0y} = 20 kPa at the beginning of the shear test were observed, and they are used as the initial values in the model prediction. From the comparison, the model provides a good prediction of the stress–strain and soil–water characteristic behaviour for this type of test. The measured and predicted results both show that the degree of saturation increases with decreasing suction during shearing under undrained conditions and constant mean net stress. It is also seen from Fig. 7a that the undrained strength of unsaturated soil can be predicted well.

Fig. 8 shows predicted and measured results for an undrained triaxial compression test on unsaturated compacted Pearl clay with a relatively high initial degree of saturation. During the test, the net lateral pressure was kept constant at 100 kPa. In order to measure the suction correctly, the axis-translation technique was adopted in the test, i.e., a constant pore air pressure of 100 kPa was applied to the specimen. As a result, a positive pore water pressure u_w was observed during shearing. Initial values of s_0 = 64.0 kPa, e_0 = 1.2, S_{r0} = 70.1% and p_{0y} = 20 kPa were observed at the beginning of the shear test, and these values were used as the initial values in the model predictions in Fig. 8. From the comparison, it is interesting to note that the model provides not only a good prediction of the stress–strain behaviour, but also the suction and degree of saturation response. Both the measurement and prediction show that the suction decreases and the degree of saturation increases during triaxial compression, with the net confining pressure being kept constant under undrained conditions.

The test results in Figs. 7 and 8 indicate that the sample with a high value of $s{\cdot}S_r$ has a higher net stress ratio at failure than the sample with a low value of $s{\cdot}S_r$ for almost the same σ_3. The model is capable of predicting this difference although the average skeleton stress ratio at failure is assumed to be the same in the model.

From Figs. 4–8, it can be seen that the model proposed by the authors well predict the coupled hydro-mechanical behaviour for both drained and undrained conditions, by using the same set of model parameters for the same clay.

5. Concluding remarks

A coupled hydro-mechanical model for unsaturated soils, reformulated for undrained conditions, has been shown to be capable of predicting the stress–strain and soil–water characteristic response. The hydro-mechanical model gives good predictions for these quantities under both drained and undrained conditions, and also gives good estimates of the undrained strength of unsaturated soils. The same set of model parameters can be used for both drained and undrained conditions for the same soil.

Acknowledgements

This research was sponsored by the National Natural Science Foundation of China Grant 10572081, the Shanghai Pujiang Program and the Innovative Foundation for graduate students at Shanghai University, China. The first-named author acknowledges the visitor's research Grant provided by Centre for Geotechnical and Materials Modelling at the University of Newcastle, Australia.

References

[1] Alonso EE, Gens A, Hight DW. Special problem soil general report. Proceedings of the ninth European conference on soil mechanics and foundation engineering 1987;3:1087–146.
[2] Alonso EE, Gens A, Josa A. A constitutive model for partially saturated soils. Geotechnique 1990;40(3):405–30.
[3] Buisson MSR, Wheeler SJ. Inclusion of hydraulic hysteresis in a new elastoplastic framework for unsaturated soils. In: Tarantino A, Mancuso C, editors. Experimental evidence and theoretical approaches in unsaturated soils; 2000. p. 109–19.
[4] Gens A, Alonso EE, Josa A. Elastoplastic modelling of partially saturated soils. Proceedings of the third international symposium on numerical models in geomechanics 1989:163–70.
[5] Karube D, Honda M, Kato S, Tsurugasaki K. The relationship between shearing characteristics and the composition of pore-water in unsaturated soil. J Geotech Eng Proc JSCE 1997;575:49–58 [in Japanese].
[6] Kohgo Y, Nakano M, Miyazaki T. Theoretical aspects of constitutive modelling for unsaturated soils. Soil Found 1993;33(4):49–63.
[7] Sheng DC, Sloan SW, Gens A. A constitutive model for unsaturated soils: thermo-mechanical and algorithmic aspects. Comput Mech 2004;33:453–65.
[8] Sun DA, Matsuoka H, Xu YF. Collapse behavior of compacted clays by suction-controlled triaxial tests. Geotech Test J ASTM 2004;27(4):362–70.
[9] Sun DA, Matsuoka H, Yao YP, Ichihara W. An elastoplastic model for unsaturated soil in three-dimensional stresses. Soil Found 2000;40(3):17–28.
[10] Sun DA, Sheng DC, Sloan SW. Elastoplastic modelling of hydraulic and stress–strain behaviour of unsaturated soils. Mech Mater 2007;39(3):212–21.
[11] Sun DA, Sheng DC, Xu YF. Collapse behaviour of unsaturated compacted soils with different initial densities. Canadian Geotech J 2007;44(6):673–86.
[12] Vaunat J, Romero E, Jommi C. An elastoplastic hydro-mechanical model for unsaturated soils. In: Tarantino A, Mancuso C, editors. Experimental, evidence and theoretical approaches in unsaturated soils; 2000. p. 121–38.
[13] Wheeler SJ, Sivakumar V. An elasto-plastic critical state framework for unsaturated soil. Geotechnique 1995;45(1):35–53.
[14] Wheeler SJ, Sharma RS, Buisson MSR. Coupling of hydraulic hysteresis and stress–strain behaviour in unsaturated soils. Geotechnique 2003;53(1):41–54.